Loss of cholesterol in Junctional Epidermolysis Bullosa skin identifies a key role for Laminin-332 in actomyosin mediated cholesterol transport

Authors and Affiliations

Eleri. M. Jones[1*], Emanuela. Camera[2], Piotr. Parzymies[1], Supatra.T. Marsh[1], Ryan.F. O'Shaughnessy[1], Monique. Aumailley[3], John. A. McGrath[4], Edel.A. O'Toole[1] and Matthew. Caley[1 *]

1. Cell Biology & Cutaneous Research, Blizard Institute, Queen Mary University of London; London, U.K.
2. Laboratory of Cutaneous Physiopathology, San Gallicano Dermatological Institute IRCCS; Rome, Italy
3. Centre for Biochemistry, Medical Faculty, University of Cologne, Cologne; Germany
4. St John's Institute of Dermatology, Kings College London (Guys Campus); London, UK

Corresponding Authors. Emails eleri.jones@qmul.ac.uk, m.caley@qmul.ac.uk

Abstract

Individuals with Junctional Epidermolysis Bullosa (JEB), a rare genetic skin disease characterised by loss of function mutations in the Laminin332 (Lam332), do not survive beyond their first birthday. Here we report that loss of Lam332 leads to absence of cholesterol lipid from the epidermis *in vitro* and *in vivo*. Stable knockdown of Lam332 chains (LAMA3, LAMB3 and LAMC2) was established using shRNA and were used to develop 3D skin equivalents. Changes in lipid synthesis were assessed by western blot analysis and immunohistochemistry. Findings were confirmed in an inducible mouse model of Lamα3 (*Lama3*$^{flox/flox}$/K14^{CreERT}) and in anonymized, archival human tissue: JEB skin and normal age-matched controls. Further lipid analysis was explored using lipidomics in 3D skin equivalents and mouse tissue. Cholesterol biosynthesis genes were increased with loss of Lam332 *in vitro*, however a decrease in nile red lipid staining was observed in Lamα3 mouse (n = 6) and in JEB patient skin (n = 7). Further changes to the epidermal lipid profile with loss of Lam332 was confirmed with lipidomic analysis of Lamα3 mouse epidermis and Lam332 skin equivalents. Cholesterol transport within Lam332 KD keratinocytes was revealed to be disrupted, which in keratinocytes is dependent on the actomyosin network, which was reversed with recombinant human Lam332. In conclusion these findings suggest a role for Lam332 in lipid metabolism in the skin and a broader role in epidermal homeostasis and barrier formation. Restoration of cholesterol transport in JEB patients offers the potential to improve the skin barrier and survival.

INTRODUCTION

Junctional Epidermolysis Bullosa (JEB) is a rare genetic skin disease characterised by skin fragility, failure to thrive and mechanically induced blistering[1]. Babies diagnosed with this form of EB generally do not survive beyond their first birthday[2]. Why this form of EB is so severe compared to recessive dystrophic epidermolysis bullosa (RDEB), despite the comparable depth of blisters and skin fragility, is poorly understood. The most severe form of JEB is caused by loss of function mutations in genes encoding the basement membrane protein Laminin332 (Lam332)[3]. Lam332 is a secreted extracellular glycoprotein composed of three genetically distinct chains α3, β3 and γ2 [4,5]. It is an essential component of the dermal-epidermal junction, acting as a bridge between the hemidesmosomes attaching the basal keratinocyte to the basement membrane and collagen type VII in anchoring fibrils anchoring the basement membrane to the dermis.

The outermost layer of the epidermis, the stratum corneum, consists of differentiated keratinocytes in a neutral lipid rich matrix. This lipid matrix has an unique organisation consisting of ceramides, cholesterol and free fatty acids, which is important for the skin's barrier function preventing water loss and entry of extrinsic pathogens [6–8].

In this study we developed a stable knockdown of each of the Lam332 chains (shLAMA3, shLAMB3 and shLAMC2) in an nTERT immortalised keratinocyte cell line to study any changes with loss of Lam332. Here we report that loss of Lam332 leads to lipid changes within the epidermis, specifically absence of cholesterol from the stratum corneum of JEB patients. The loss of skin cholesterol is due to a defect in cholesterol transport, which in keratinocytes we identify to be dependent on the actomyosin network, which is disrupted by loss of Lam332. In conclusion these findings suggest a role for Lam332 in lipid metabolism in the skin and a broader role in epidermal homeostasis and barrier formation. Restoration of cholesterol transport in JEB patients offers the potential to improve the skin barrier and survival.

RESULTS

Loss of Laminin332 upregulates cholesterol biosynthesis genes

The α3 subunit of Lam332 was successfully knocked down with siRNA in primary keratinocytes (Supplementary Fig. 1a) with greater than 95% down-regulation compared to controls. Analysis by RNAseq, comparing these cells to siControl cells, generated a dataset of differentially expressed genes. Over representation analysis of this dataset (DAVID GO Terms, Supplementary Table. 1) identified a subset of genes involved in lipid biosynthesis that were significantly overrepresented in the siLamα3 gene list (Fig. 1a and b).

These observations were confirmed by generating stable knockdowns of each chain of Lam332 (shLAMA3, shLAMB3 and shLAMC2; Supplementary Fig. 2a) in an nTERT immortalised keratinocyte cell line. Upregulation of cholesterol biosynthesis pathway genes (*HMGCS1, HMGCR, MVD, LSS, FDPS, NSDHL, DHCR7* and *DHCR24*) was confirmed by real-time qPCR (Fig. 1c). The increase in *HMGCS1*, *HMGCR*, *MVD* and *LSS* was confirmed at protein level by western blotting (Fig. 1d) and immunofluorescence (Fig. 1e). 3D skin equivalent cultures were generated with shC, shLAMA3, shLAMB3, shLAMC2 and siC and siLAMA3 keratinocytes and validated for loss of each Lam332 chain (Supplementary Fig. 2b and 1b). Cholesterol biosynthesis genes were upregulated in the 3D skin equivalent models simulating JEB (Fig. 1f and Supplementary. 1b). Loss of the basement membrane protein Collagen type VII, which results in another blistering disease RDEB [9,10] did not cause any changes (Supplementary Fig 3a).

An inducible mouse model of Lamα3[11] (*Lama3*$^{flox/flox}$/K14^{CreERT} mouse; KO) also showed changes in cholesterol biosynthesis genes. Immunostaining of skin sections from these mice revealed an upregulation of *Hmgcs1*, *Hmgcr* and *Mvd* compared to control (Ctrl) *Lama3*$^{wt/flox}$/K14^{CreERT} mouse (Fig. 3a). Moreover, expression of cholesterol biosynthesis genes was increased in both *LAMA3* (n=4) and *LAMB3* (n=3) mutant JEB patient samples compared to control skin (n=5) (Fig. 3b), relevant to human disease. Patient details are in Supplementary Table 2.

Loss of Laminin332 results in changes in skin lipids

Nile red staining of siLamα3 skin equivalents (Supplementary Fig.1b), *Lama3* KO mouse (Fig. 3c) and JEB patient skin (Fig. 3d) revealed reduced polar and non-polar (barrier) lipids compared to respective controls. In contrast no loss of lipid barrier was observed with knockdown of Collagen VII (Supplementary Fig 3b). A loss of barrier function was demonstrated in siLamα3 skin equivalents with failure to retain Lucifer yellow dye compared to siC (Supplementary Fig. 1b). To explore the epidermal lipid profile with loss of Lam332 we performed GC-MS in conjunction with untargeted/targeted LC-MS of *Lama3* mouse epidermis and Lam332 skin equivalents. Untargeted LC-MS demonstrated substantial differences in comprehensive lipid profiles between control and *Lama3* KO mouse epidermal extracts in both positive (Fig. 3) and negative (Supplementary Fig. 4) ion mode (+/-ESI). Volcano plot analysis revealed significantly different lipid entities between samples with a fold change higher than 1.5 (Fig. 3b and Supplementary Fig 4b). Targeted analyses indicated a downregulation of glycerolipids, and a small percentage of sphingolipids and phospholipids in the *Lama3* KO compared to control mouse. In contrast, sphingolipids accounted for most upregulated lipids, followed by wax esters, glycerolipids, ethanolamines and phospholipids (Fig. 3c, d and Supplementary Fig. 4c). Cholesterol esters (CE) and cholesterol sulfate (CS) were quantitatively determined by LC-MS whereas cholesterol and desmosterol were analysed from the same lipid extracts by GC-MS. No significant changes were observed in cholesterol and desmosterol, but a significant upregulation of CS and downregulation of CE(18:1) was observed in the *Lama3* KO epidermis (Fig. 4e-h).

Similarly, analysis of Lam332 skin equivalents revealed considerable differences in the lipid profiles compared to control (Supplementary Fig 5a, b). Several species were universally modulated between the three laminin knockdown subtypes, 5 were commonly downmodulated and 23 were commonly upmodulated (Supplementary Fig.5c, d). However, each laminin chain knockdown resulted in variable lipid changes, specifically for the phospholipid sub-class (e.g. phosphatidylglycerol (PG), phosphatidylethanolamine (PE), phosphatidylinositol (PI)) (Supplemantary Fig. 5b, e). Quantitative analysis of cholesterol metabolites in skin equivalents revealed a significant upregulation of CS in the Lam332 knockdown samples (Supplementary Fig 5f-i).

Loss of Laminin332 results in disrupted transport of cholesterol.

Total cholesterol (TC) remained unchanged (Supplementary Fig. 6a) but CE was decreased (Supplementary Fig. 6b) with loss of Lam332 in cultured keratinocytes and loss of cholesterol in the epidermis (Supplementary Fig. 2b and 3b), suggesting abnormal cholesterol transport. Uptake of LDL with loss of Lam332 was investigated by monitoring the binding and internalisation of 1,1′-dioctadecyl-3,3,3′,3′-tetramethylindo-carbocynanine perchlorate (dil-LDL) in Lam332 knockdown cells. There was no difference in LDL binding (Supplementary Fig. 6c & d) or LDL receptor expression in any of the cell lines (Supplementary Fig.6f). However, LDL uptake was significantly increased in Lam332 KD cells (Supplementary Fig.6c and e); suggesting a failure of the LDL to be recycled efficiently and therefore an accumulation within the cell. Furthermore, analysis of the LDL-receptor showed an accumulation of the precursor form (Supplementary Fig. 6f), suggesting an issue with the recycling of the mature receptor.

To further assess the transport of cholesterol within Lam332 knockdown cells, we imaged the movement of fluorescent dil-LDL and EGF by time lapse video microscopy over a 2-hour period. It showed reduced movement of dil-LDL in Lam332 knockdown cells compared to control (Supplementary Video 1-4), but no change in EGF movement (Supplementary Video 9-12). Particle tracking analysis on representative videos showed a significant reduction in LDL movement which was reversed when cells were cultured on hrLam332 (Supplementary Video 5-8) (Fig. 4a). EGF movement, controlled by microtubules[12], was unchanged in Lam332 knockdown cells (Fig. 4b), suggesting that cholesterol is transported within the cell through a different mechanism.

To further explore this defect in cholesterol transport, we investigated the proteins involved in the intracellular cholesterol transport pathway in shLamA3 keratinocytes. Our analysis demonstrated that the levels of NPC2 and Myo5b were downregulated in shLAMA3 compared to shC (Fig. 4f and g), with a subsequent restoration when the cells were cultured on hrLam332. Interestingly, this restoration appeared to be more pronounced for Myo5b than NPC2 suggesting a potential time-dependent effect of the recombinant protein. Levels of NPC1, an NPC2-binding partner, were upregulated in

shLAMA3 (Fig.4f) suggesting a potential compensatory mechanism. Myo5b partners, rab8a and rab11a (which regulate cholesterol recycling) were expressed at similar levels in shC and shLAMA3 keratinocytes (Fig.4f).

Cholesterol movement is dependent on the actin cytoskeleton network.

The actin cytoskeleton was analysed in Lam332 knockdown skin equivalents with phalloidin revealing a reduced intensity of filamentous actin throughout the epidermis, with a marked absence at the basement membrane, in all Lam332 knockdown skin equivalents (Fig. 4c). Furthermore, filipin staining revealed a significant reduction in plasma membrane cholesterol in Lam332 knockdown cells compared to control, which was restored to control levels when cells were cultured on hrLam332 (Fig. 4d and e, Supplementary Fig.7). To verify whether cholesterol transport from the ER to the plasma membrane (PM) is dependent on the actin cytoskeleton we disrupted the actomyosin network, which revealed that cholesterol transport to the PM is dependent on the actin cytoskeleton as was visualised by the loss of PM cholesterol staining in control (shC) cells treated with blebbistatin and latrunculin B (Fig. 4d). This loss of cholesterol at the PM was not restored with hrLam332 (Fig. 6e).

Plasma membrane levels of the transmembrane β1 integrin in both of our cell lines grown on BSA and hrLam332 demonstrated a statistically significant decrease of integrin β1 in the shLamA3 knockdown cells which was partially restored by the addition of hrLam332 (Supp Fig. 8). The levels of both total and activated (y397) FAK were decreased in our shLAMA3 keratinocytes with a complete restoration when the cells were grown on hrLam332 (Supp Fig. 8).

DISCUSSION

Laminin332 is an important component of the skin basement membrane, which is absent in JEB skin resulting in defective epidermal-dermal adhesion where patients suffer from severe blistering from birth[1]. The extracellular hydrophobic lipid matrix of the epidermal stratum corneum provides a barrier, preventing water loss and entry of extrinsic pathogens and allergens[13–16]. We identify for the first time that loss of Lam332 seen in JEB, but not loss of Collagen type VII (Supplementary Fig 3), leads to an

altered epidermal lipid profile due to changes in cholesterol transport. Specifically, loss of Lam332 from the basement membrane disrupts the filamentous actin network within basal keratinocytes and we demonstrate that actin-myosin transport is the major mechanism for cholesterol transport in keratinocytes. These findings suggest that an impaired skin barrier due to loss of epidermal lipids may contribute to infection and disease severity of JEB when compared to other forms of EB such as RDEB.

Depletion of stratum corneum lipids are associated with numerous skin diseases including atopic dermatitis (AD)[17], ichthyosis[18], xerosis[19], acne vulgaris[20,21] and aged dry skin[22]. Significant changes in epidermal lipids lead to an increase in trans epidermal water loss (TEWL) and barrier dysfunction in the epidermis[16], reducing the skin's ability to protect the body from external infections. Furthermore, lipids are considered important multifunctional mediators that influence the process of epidermal metabolism, inflammation, cell proliferation and differentiation[23].

Lipidomic analysis revealed significant changes in epidermal lipids in both mouse and 3D skin equivalents with loss of Lam332. Although both disease models resulted in distinct lipid changes within the epidermis, both offer an insight into the role of Lam332 in formation of the lipid barrier. The *Lama3* KO mouse revealed a significant upregulation in sphingolipids. Ceramides are considered key in epidermal barrier maintenance[24,25] and in regulating keratinocyte proliferation, differentiation and apoptosis[26]. Ceramides have been extensively studied in psoriasis, AD and ichthyoses[25]. An increase in specifically short chain ceramides was observed which has previously been shown to limit formation of an efficient lipid barrier in AD[27]. In the skin equivalent model however, it was changes in phospholipids that were highlighted with loss of Lam332. Phospholipids are essential for cellular dynamics[28] and alterations may affect the epidermal barrier[29]. Significant changes in phospholipids have previously been associated with AD[30]. Evidence has shown that an increase in ceramides regulates cholesterol metabolism and reduces its translocation,[31] and can also alter membrane dynamics reorganising the lipid domain resulting in actin cytoskeleton remodelling[32,33]. This imbalance of membrane lipids could have a significant effect on the defensive role lipids play in the epidermal barrier of the skin[34].

Cholesterol is an important regulator of lipid organisation, and a complex cellular mechanism is required to maintain cholesterol levels in membranes[35]. A significant reduction in CE led to the discovery that cholesterol transport with loss of Lam332 was significantly impaired. Despite extensive research into Niemann-Pick disease, the most common cholesterol transport disorder[36], there remains unresolved questions on how cholesterol moves within cells and how it is exported. In inflammatory skin diseases such as psoriasis, evidence has shown a role for cholesterol in IL17A signalling[37]. Furthermore, evidence suggests that lipid metabolism and cholesterol trafficking directly regulate the inflammatory pathways in macrophages[38]; suggesting that cholesterol could have multiple roles within the skin providing an adequate lipid barrier as well as maintaining the inflammatory response.

We describe for the first time that loss of Lam332 at the basement membrane directly results in defective transport of cholesterol in the epidermis due to instability of the actomyosin network. While the intracellular cholesterol transport towards the plasma membrane has been widely studied in other cell lines including; squamous cell carcinoma (A431)[39] rat hepatoma (CRL-1601) cell line[40], Chinese hamster ovary cells[41], fibroblasts[42,43] including human skin fibroblasts[44] the molecular mechanisms in skin keratinocytes are poorly understood[45]. We show that in keratinocytes, cholesterol movement is dependent on vesicle transport driven by the actin cytoskeleton. We further delved into the cholesterol transport pathway, briefly, extracellular cholesterol (carried by LDL) is internalised by the cell in the process of receptor-mediated endocytosis and subsequently de-esterified in the early endosome. Free cholesterol is transferred by the soluble NPC2 protein to the endosome membrane bound NPC1. The cargo is then delivered back to the plasma membrane by the activity of Rab8a or Rab11a GTPases and the actin bound Myo5b[39,46,47]. Myo5b has a well-known role in the final stages of cholesterol recycling[39], whereby its deletion in a 3D human skin model perturbed the epidermal barrier function leading to a decrease in epidermal lipids and cell-cell junction proteins[47]. Furthermore, Myo5b KO mice show extensive wrinkling, characteristic of a defective epidermal barrier[48]. We did not observe downregulation of rab8a or rab11a in our knockdown cell line suggesting that the cell's ability to produce lipid-transporting vesicles such as lamellar bodies is not compromised and that our phenotype is likely due to the cell's inability to transport those vesicles efficiently.

Cholesterol recycled by actin dependent Myo5b has been shown to be preferentially delivered to the sites of focal adhesions[39]. Focal adhesion kinase (FAK) is a key component of focal adhesions playing a crucial role in the stabilisation of the actin cytoskeleton[49]. Our results demonstrated that shLAMA3 keratinocytes had lower levels of FAK (both total and activated, Supp. Fig 8), as well as lower levels of plasma membrane integrin β1, which is known to act as a Lam332 binding partner and is an important component of focal adhesions[50]. JEB patient keratinocytes show aberrant formation of actin containing focal adhesions[51], and an abnormal distribution of integrin α6β4 along the basement membrane of JEB patient skin[52,53]. Lam332 is an important adhesion molecule, which along with integrin α6β4 and α3β1, BPAG2, and plectin[54], contribute to anchorage of keratinocytes and formation of the hemidesmosome. Disruption of any of the Lam332 genes result in destabilisation of the hemidesmosome and importantly the cytoskeletal networks[55]. These results corroborate previous findings that loss of Lam332 results in a disrupted actin cytoskeleton[56].

There is no cure for patients with JEB, while current treatment is aimed only at palliative care[57]. One extreme treatment for JEB generalised severe was the regeneration of the entire skin epidermis in a patient with a mutation in *LAMB3*[58]*.* Therefore, potential treatment aimed at increasing the cholesterol within the epidermis could restore the lipid defect within the epidermis of JEB skin. This would not prevent severe blistering or reverse skin fragility but could extend patient lifespan by reducing the occurrence of infections due to the severe barrier defect. Through investigating the loss of Lam332 in JEB we reveal an important role for the basement membrane in regulation of cholesterol transport and epidermal barrier, this could be significant for JEB and skin ageing.

MATERIALS AND METHODS

Cell Culture

The immortalised n-TERT keratinocyte cell lines were cultured in DMEM:Ham's F12 (3:1) supplemented with 10% FCS, 1% L-glutamine (200 mM) and RM Plus (0.4 µg/ml hydrocortisone, 5 µg/ml insulin, 10 ng/ml EGF, 5 µg/ml transferrin, 8.4 ng/ml cholera toxin, and 13 ng/ml liothyronine). Human dermal fibroblasts (HF) were cultured in DMEM

supplemented with 10% FCS and 1% L-glutamine (200 mM). All cells were cultured at 37°C and 5% CO_2.

Generation of shRNA-Transduced Cell Lines

For stable knock-down of Laminin332 chains, α3, β3 and γ2 in keratinocytes, the nTERT keratinocyte cell line was transduced with SMARTvector™ lentiviral particles (Thermo Fisher Scientific, Paisley, UK) of three different shRNA clones (Supplementary Table S3) targeting either laminin chains as well as non-targeting particles (negative control). N-TERT keratinocyte cells, seeded at 50% confluency, were incubated overnight with viral particles at a MOI (multiplicity of infection) of 2 diluted in complete DMEM:Ham's F12 media supplemented with polybrene (5 µg/ml). Transduced cells were selected in puromycin (2.5 µg/ml) 48 hours after.

siRNA Transfection

For Laminin- α3 chain knockdown, the nTERT keratinocyte cell line was transfected with a SMARTpool of four synthetic siRNAs (Dharmacon, UK), targeting the α3 chain (Supplementary Table) or non-targeting siRNAs (siC) as a negative control. Cells were plated at 60% confluency and transfected with 4µg of Dharmafect1 (Thermo Fisher Scientific) transfection reagent and 12.5nM final concentration of each siRNA.

***In vitro* epidermal models**

Skin equivalent cultures using a Collagen:matrigel gel were prepared by mixing 4.9 volumes of type I collagen (BD Biosciences, Oxford, UK), 2.1 volumes of Matrigel (BD Biosciences), 1 volume of 10x MEM, 1 volume of FCS, and 1 volume of DMEM/10% FCS/HF (resuspended at a density of $1x10^6$/ml) and adding onto cell culture insert (0.4um pore size, Corning). Gels were incubated for 1 hour to equilibrate and then keratinocytes (shC, shLamA3, shLamB3 and shLamC2) were seeded on the top of the gel at a density of $3.4x10^5$ per gel. After 24 hours, gels were raised to the air-liquid interface. Ascorbic acid was added to the media at a concentration of 50µM/mL from day 7 and media replaced every day. The gels were harvested 14 days after, either fixed in 4% PFA and embedded in paraffin or embedded in OCT and frozen.

Protein Analysis

For cell lysate immunoblot analysis, keratinocytes were lysed in 1x RIPA buffer (details) supplemented with a protease-inhibitor-cocktail (Roche, Burgess Hill, UK). Lysates were subjected to 10% SDS-PAGE. The presence of protein was detected by immunoblotting using a primary antibody at 4°C overnight, and a horseradish peroxidase-coupled anti-mouse or -rabbit secondary antibody for 1 hour at room temperature and developed using Enhanced Chemi Luminescence. For densitometry analysis, the image analysis program Image J was used.

qRTPCR

RNA extraction was performed using the RNeasy mini kit (Qiagen, Manchester, UK) according to the manufacturer's instructions. cDNA was generated using the SuperScript® VILO™ cDNA Synthesis kit (Invitrogen, Paisley, UK). qPCR was carried out using KAPA SYBR® Universal qPCR Mastermix (Anachem, Luton, UK) on a StepOnePlus Real-Time PCR System (Thermo Fisher Scientific). Primer sequences are shown in Supplementary Table S4.

Cholesterol quantification

Total cholesterol (TC) and free cholesterol (FC) were determined using the Cholesterol/Cholesteryl Ester Quantitation Assay (Abcam plc., Cambridge, UK), according to the manufacturer's protocol. Briefly, samples (1 x 10^6 cells) were extracted with 200 µl of chloroform:isopropanol:NP-40 (7:11:0.1) using a microhomogenizer. After centrifugation at 13,000g for 10 min to remove insoluble material, the organic phase of samples was transferred to a new tube and dried in a vacuum for 30 min to remove chloroform. Dried lipids were then dissolved with 200 µl of the Cholesterol Assay Buffer. Fifty microlitres of samples and standards (1–5 ng) were added to 200µl of reaction mixture after 60 min incubation at 37°C the OD was measured at 570nm by a ELISA-reader. Cholesterol esters (CE) were determined by subtracting the value of FC from the TC.

Filipin Fluorescence Staining

A cell-based Cholesterol Assay Kit from Abcam (Cambridge, UK) was performed in keratinocyte cells in order to visualize cholesterol by using Filipin III as a fluorescence probe of cholesterol. Briefly, 20,000 cells were seeded on glass coverslips in a 24 well plate and

cultured in DMEM/F12 for 48 hours. After removal of culture medium from wells, cells were washed with PBS and fixed for 10 min and washed (3 x 5 min). Filipin III solution was added to each well assayed and maintained in the dark for 45 min at room temperature. After washing (2 x 5 min) fluorescence images were obtained using 40x oil objective.

Fluorescence and Immunostaining

Skin sections were obtained of frozen human JEB and normal skin. Five μm-thick cryosections from skin equivalent cultures were cut in a cryostat, air-dried and fixed in 4% paraformaldehyde for 10 minutes before staining. Five μm-thick paraffin sections were de-paraffinized using xylene, hydrated in descending grades of ethanol to distilled water, and antigen retrieval was performed by heating samples in boiling 10 mM citrate buffer, pH 6.0, for 10 minutes.

Sections from skin equivalent cultures or patient skin were blocked at room temperature by incubating in blocking buffer (1% BSA (w/v) 2% FCS (v/v)) for 1 hour. Incubation with the primary antibody (see Supplementary Table S5) diluted in blocking buffer was performed at 4°C overnight. The secondary Alexa Fluor 568-red or 488-green, goat anti-rabbit or goat anti-mouse antibodies were added at a 1:250 dilution for 1 hour at room temperature. DAPI (300nM) was used as a nuclear stain. Images were photographed using a Leica DM4000 epifluorescence microscope. Images were analysed using ImageJ and CellProfiler.

Dil-LDL binding and uptake

Cells were incubated with 5μg/ml of dil-LDL for 30 minutes at 4˚C (binding) or 30 minutes at 37˚C (uptake) in epilife medium prior to fixation with 4% PFA and staining with DAPI for detection of nuclei. Images were taken on the Incell 2200 microscope and dil-LDL intensity was quantified. The total intensity for dil-LDL was divided by the number of nuclei per image to obtain an intensity per cell value.

Cells were seeded (3000 per well) in a 96 well plate, either coated with BSA or recombinant Laminin332 (BioLamina LN332-0502, diluted in Dulbecco's Phosphate Buffered Saline, Sigma, D8662) and left to adhere overnight. Cells were starved of cholesterol for 24hrs in epilife culture media. Fluorescent dil-LDL was added at dilution of 1:200 for 10mins, cells were washed repeatedly with PBS-heparin (to remove any surface bound LDL). They were then incubated with DRAQ5 (nuclear dye) and ER-tracker in epilife media for live imaging. Cells were imaged at 40x every 4 minutes for 2 hours using the InCell 2200 and videos created with

the software. LDL movement was tracked using ICY software and an average of 20 images analysed.

Actin disruption

Cells seeded onto coverslips coated with either BSA or recombinant Laminin332 were treated with blebbistatin (25µm) or latrunculinB (1µm) for 24 hours before being fixed and stained with filipin to visualise plasma membrane cholesterol.

Flow cytometry

Cells were seeded at 200,000 cells in a T25 flask coated with 3 ml of 5µg/mL of BSA or hrLam332 (as previous) and incubated for 48 hours. Cells were trypsinised and 50,000 cells were placed in each FACS tube, centrifuged for 5min at 380g at 4°C. The supernatant was discarded, and the cells were resuspended in PBS containing APC mouse anti-human integrin-β1 antibody or the IgG1 K isotype control (1:100 dilution) and incubated for 15 minutes. 500µl of PBS was added to each tube, the cells were centrifuged in the same conditions and the supernatant was discarded. The cells were then resuspended in 300µl of DAPI dissolved in PBS (1:2,000) and analysed immediately using the BD FACS Canto II Flow Cytometry system. The geometric mean of plasma membrane integrin β1 intensity per single cell was then calculated using the FlowJo software and corrected for non-specific background signal using the isotype controls and DAPI only samples as negative controls.

Sample processing for the analysis of epidermal lipids.

For mouse samples (control n=6 and *Lama3* KO n=6), the epidermis was separated from the dermis by placing whole skin sections in dispase solution overnight at 4˚C, while skin equivalents (shC n=3, shLAMA3 n=3, shLAMB3 n=3 and shLAMC2 n=3) were treated whole. Mouse epidermis or skin equivalents were weighed and lipids extracted with a chloroform/methanol mixture 2:1 after addition of the internal standard mixture containing SPLASH Lipidomix®,-LM6002 and d31Cer[NS] 34:1 (Avanti Polar Lipids, USA), and in-house mixed deuterated standards supplied by C/D/N isotopes and Toronto Research Chemicals, both from Canada (see Supplementary Table S6). Aliquots of dissolved lipid extracts were analysed by GC-MS for the quantification of cholesterol, desmosterol and free fatty acids. The dissolved lipid extracts were further analysed by untargeted LC-MS in positive and negative ion mode. The results of the untargeted approach were normalised by the internal standard

d31Cer[NS] 34:1 and the weight of each sample. Quantitative results from both GC-MS and LC-MS were normalized by the mg of tissue weight and reported as pmol/mg.

Gas chromatography-mass spectrometry

Gas chromatography coupled to electron ionization mass spectrometry (GC-MS) dual scan-selected ion monitoring was employed to determine quantitatively target compounds in the lipid extracts. Samples were analyzed with a GC 7890A coupled to the MS 5975 VL analyzer (Agilent Technologies, CA, USA). Quantitative analysis of sterols was performed as previously reported (Singh K, 2018). Briefly, dissolved lipid extracts were dried under nitrogen and derivatized with 50 µL BSTFA added with 1% trimethylchlorosilane (TCMS) in pyridine. To generate the trimethylsilyl (TMS) derivatives of sterols, the reaction was carried out at 60 °C for 60 minutes. GC separation was performed with the 30 m–0.250 (i.d.) GC DB-5MS UI fused silica column (Agilent Technologies, CA, USA), chemically bonded with a 5% diphenyl 95% dimethylpolysiloxane cross-linked stationary phase (0.25 mm film thickness). Helium was used as the carrier gas. Samples were acquired in scan mode by means of electron impact (EI) MS. Cholesterol and desmosterol were determined against d7cholesterol and d6desmosterol, respectively, with the MassHunter quantitative software (Agilent Technologies, CA, USA).

Liquid chromatography-mass spectrometry

The chromatographic apparatus consisted of the 1260 Infinity II series LC system (Agilent Technologies, CA, USA). The stationary phase of the high-resolution reversed phase LC was a Zorbax SB-C8 Zorbax SB-C8 rapid resolution HT 2.1 x 100 mm 1.8 µm p.s. with a maximal operational backpressure at 600 Bar (Agilent Technologies, CA, USA). Lipid mixtures were eluted with a gradient of (A) 5 mM ammonium formate in water, (B) methanol, (C) acetonitrile, (D) isopropanol. The mobile phases were filtered through 0.45 µm glass filters and continuously degassed under vacuum. The elution program was as follows: A/B/C/D 60/28/8/40 at time 0 and held for 1 min, brought to A/B/C/D 1/70/20/9 in 10 min and held up to 20 min. The flow rate was maintained at 400 µL/min during the entire LC run. The column was thermostated at 60 ºC. The injection volume was 0.20 µL. The injector needle was washed with the mobile phase in the wash port during the LC runs. The eluent outlet was connected to two different MS analyzers for the detection and characterization.

Accurate mass measurements in full MS and auto MS/MS were conducted with a G6545B series hyphenated QTOF (Agilent Technologies, USA) equipped with a JetStream Technology electrospray interface (ESI) operating in both positive and negative ion mode. Analytes eluted from the LC system were introduced into the Q-TOF apparatus at the operating

chromatographic flow rate (see chromatographic conditions). Nitrogen was used as the nebulizing and desolvation gas. The temperature and the flow of the drying gas temperature were 200 °C, and 12 L/min, respectively. The temperature and the flow of the sheath gas were 350°C and 12 L/min, respectively. The nebulizer pressure was 40 psi. The capillary and the fragmentor voltage were 4000 and 180 V, respectively. Full scan mass spectra were acquired in the positive and negative ion modes in the range from m/z 100 to m/z 1600. To enhance accurate mass measurement for the ion species a reference solution of two compounds with m/z 121.050873 and 922.009798, in positive ion mode and m/z 112.995587 and 966.000725 in negative ion mode, was vaporized in continuum in the spray chamber by means of a separate nebulizer.

Extraction of MS features

Molecular features, defined by an m/z, ration, retention time (RT) and signal intensity value, were extracted in profile mode within the 10 ppm mass window from the raw LC-MS data files using the untargeted or the targeted batch recursive feature extraction in the MassHunter Profinder software (Agilent Technologies, USA). Procedures and details can be found in 'MassHunter Profinder Software Quick Start Guide. G3835-90027_Profinder_QuickStart' on the Agilent Technologies webpage. The features extracted were exported into a compound exchange format (CEF) reporting RT, the accurate mass and the absolute abundance for each entity to be processed in the subsequent chemometric analysis as previously reported [59,60].

Data analysis

Agilent Mass Profiler Professional (MPP version 15.1) was used to process the LC-MS untargeted and targeted data. RT were aligned by setting a RT window of 0.6 minutes, whereas m/z binning was performed by setting windows at 10 ppm. Absolute abundance of each entity was normalized by the absolute abundance of the d31Cer[NS] 34:1 internal standard. Data were filtered by frequency of detection, which reflects the number of samples that presented particular features. A frequency filter was applied to data extracted from MPP and only entities present in 100% of samples belonging to at least one of the investigated groups were retained for the statistical analysis. Fold changes of filtered entities were compared between groups volcano plots in the MPP tools. Fold changes with p values < 0.05 after the Bonferroni's correction were considered as significant. Identification of entities within the MPP workflow was performed based on the METLIN Metabolomics Database (http://metlin.scripps.edu/) and the Lipid Annotator software (Agilent Technologies, CA, USA). Quantitative assessments of cholesterol sulfate and CE were performed with the labelled internal standards d7CHS, and d7CE (18:1), respectively.

Supplementary Materials

References

1. Varki, R., Sadowski, S., Pfendner, E. & Uitto, J. Epidermolysis bullosa. I. Molecular genetics of the junctional and hemidesmosomal variants. **43**, (2006).

2. Hammersen, J. *et al.* Genotype, Clinical Course, and Therapeutic Decision Making in 76 Infants with Severe Generalized Junctional Epidermolysis Bullosa. *J. Invest. Dermatol.* **136**, 2150–2157 (2016).

3. Kiritsi, D., Has, C. & Bruckner-Tuderman, L. Laminin 332 in junctional epidermolysis bullosa. *Cell Adh. Migr.* (2013) doi:10.4161/cam.22418.

4. Miner, J. H. & Yurchenco, P. D. Laminin functions in tissue morphogenesis. *Annual Review of Cell and Developmental Biology* vol. 20 255–284 (2004).

5. Timpl, R. & Brown, J. C. The laminins. *Matrix Biology* vol. 14 275–281 (1994).

6. Pappas, A. Epidermal surface lipids. *Dermatoendocrinol.* **1**, 72–6 (2009).

7. Feingold, K. R. The outer frontier: the importance of lipid metabolism in the skin. *J. Lipid Res.* **50 Suppl**, S417-22 (2009).

8. Feingold, K. & Elias, P. The important role of lipids in the epidermis and their role in the formation and maintenance of the cutaneous barrier. *Biochim. Biophys. Acta - Mol. Cell Biol. Lipids* **1841**, 279 (2014).

9. Uitto, J. & Christiano, A. M. Molecular basis for the dystrophic forms of epidermolysis bullosa: mutations in the type VII collagen gene. *Arch. Dermatological Res. 1995 2871* **287**, 16–22 (1994).

10. Chung, H. J. & Uitto, J. Type VII Collagen: The Anchoring Fibril Protein at Fault in Dystrophic Epidermolysis Bullosa. *Dermatologic Clinics* vol. 28 93–105 (2010).

11. Pesch, M., König, S., Aumailley, M., Kö Nig, S. & Aumailley, M. Targeted Disruption of the Lama3 Gene in Adult Mice Is Sufficient to Induce Skin Inflammation and Fibrosis. *J. Invest. Dermatol.* **137**, 332–340 (2017).

12. Crossley, L., Garrett, C. A., Hafezparast, M. & Madzvamuse, A. From the Cell Membrane to the Nucleus: Unearthing Transport Mechanisms for Dynein. *Bull. Math. Biol.* **74**, 2032–2061 (2012).

13. Elias, P. M. & Menon, G. K. Structural and lipid biochemical correlates of the epidermal permeability barrier. *Advances in lipid research* vol. 24 1–26 (1991).

14. Feingold, K. R. Thematic review series: skin lipids. The role of epidermal lipids in cutaneous permeability barrier homeostasis. *J. Lipid Res.* **48**, 2531–46 (2007).

15. Feingold, K. R. & Elias, P. M. Role of lipids in the formation and maintenance of the cutaneous permeability barrier. *Biochim. Biophys. Acta - Mol. Cell Biol. Lipids* **1841**, 280–294 (2014).

16. Jia, Y., Gan, Y., He, C., Chen, Z. & Zhou, C. The mechanism of skin lipids influencing skin status. *J. Dermatol. Sci.* **89**, 112–119 (2018).

17. Proksch, E., Jensen, J. M. & Elias, P. M. Skin lipids and epidermal differentiation in atopic dermatitis. *Clinics in Dermatology* vol. 21 134–144 (2003).

18. Zettersten, E. *et al.* Recessive x-Linked Ichthyosis: Role of Cholesterol-Sulfate Accumulation in the Barrier Abnormality. *J. Invest. Dermatol.* **111**, 784–790 (1998).

19. Akimoto, K., Yoshikawa, N., Higaki, Y., Kawashima, M. & Imokawa, G. Quantitative analysis of stratum corneum lipids in xerosis and asteatotic eczema. *J. Dermatol.* **20**, 1–6 (1993).

20. Cunliffe, W. J., Cotterill, J. A., Williamson, B. & Forster, R. A. The Relevance of Skin Surface Lipids to Acne Vulgaris. *Br. J. Dermatol.* **86**, 10–15 (1972).

21. Pappas, A., Johnsen, S., Liu, J.-C. & Eisinger, M. Sebum analysis of individuals with and without acne. *Dermatoendocrinol.* **1**, 157–161 (2009).

22. Jin, K. *et al.* Analysis of beta-glucocerebrosidase and ceramidase activities in atopic and aged dry skin. *Acta Derm. Venereol.* **74**, 337–340 (1994).

23. De Luca, C., Valacchi, G. & Wertz, P. W. Surface Lipids as Multifunctional Mediators of Skin Responses to Environmental Stimuli. *Mediators Inflamm.* **2010**, (2010).

24. Breiden, B., Sandhoff, K., Feingold, K. R. & Elias, P. The role of sphingolipid metabolism in cutaneous permeability barrier formation ☆. (2014) doi:10.1016/j.bbalip.2013.08.010.

25. Borodzicz, S., Rudnicka, L., Mirowska-Guzel, D. & Cudnoch-Jedrzejewska, A. *The role of epidermal sphingolipids in dermatologic diseases*. *Lipids in Health and Disease* vol. 15 13 (BioMed Central Ltd., 2016).

26. Uchida, Y. Ceramide signaling in mammalian epidermis. *Biochimica et Biophysica Acta - Molecular and Cell Biology of Lipids* vol. 1841 453–462 (2014).

27. Janssens, M. *et al.* Increase in short-chain ceramides correlates with an altered lipid

organization and decreased barrier function in atopic eczema patients. *J. Lipid Res.* **53**, 2755–2766 (2012).

28. Suetsugu, S., Kurisu, S. & Takenawa, T. Dynamic Shaping of Cellular Membranes by Phospholipids and Membrane-Deforming Proteins. *Physiol. Rev.* **94**, 1219–1248 (2014).

29. Han, X. Lipidomics for studying metabolism. *Nature Reviews Endocrinology* vol. 12 668–679 (2016).

30. Schafer, L. & Kragballe, K. Abnormalities in epidermal lipid metabolism in patients with atopic dermatitis. *J. Invest. Dermatol.* **96**, 10–15 (1991).

31. Subbaiah, P. V., Sowa, J. M. & Singh, D. K. Sphingolipids and cellular cholesterol homeostasis. Effect of ceramide on cholesterol trafficking and HMG CoA reductase activity. *Arch. Biochem. Biophys.* **474**, 32–38 (2008).

32. Gupta, A., Muralidharan, S., Torta, F., Wenk, M. R. & Wohland, T. Long acyl chain ceramides govern cholesterol and cytoskeleton dependence of membrane outer leaflet dynamics. *Biochim. Biophys. Acta - Biomembr.* **1862**, 183153 (2020).

33. Zeidan, Y. H., Jenkins, R. W. & Hannun, Y. A. Remodeling of cellular cytoskeleton by the acid sphingomyelinase/ceramide pathway. *J. Cell Biol.* **181**, 335–350 (2008).

34. Feingold, K. R. & Jiang, Y. J. The mechanisms by which lipids coordinately regulate the formation of the protein and lipid domains of the stratum corneum: Role of fatty acids, oxysterols, cholesterol sulfate and ceramides as signaling molecules. *Dermatoendocrinol.* **3**, 113–8 (2011).

35. Maxfield, F. R. & Tabas, I. Role of cholesterol and lipid organization in disease. (2005) doi:10.1038/nature04399.

36. Mukherjee, S. & Maxfield, F. R. Lipid and cholesterol trafficking in NPC. *Biochimica et Biophysica Acta - Molecular and Cell Biology of Lipids* vol. 1685 28–37 (2004).

37. Varshney, P. *et al.* Transcriptome profiling unveils the role of cholesterol in IL-17A signaling in psoriasis. *Nat. Publ. Gr.* (2015) doi:10.1038/srep19295.

38. de la Roche, M. *et al.* Trafficking of cholesterol to the ER is required for NLRP3 inflammasome activation. *J. Cell Biol.* jcb.201709057 (2018) doi:10.1083/jcb.201709057.

39. Kanerva, K. *et al.* LDL Cholesterol Recycles to the Plasma Membrane via a Rab8a-Myosin5b-Actin-Dependent Membrane Transport Route. *Dev. Cell* **27**, 249–262

(2013).

40. Chu, B. B. *et al.* Requirement of myosin Vb.Rab11a.Rab11-FIP2 complex in cholesterol-regulated translocation of NPC1L1 to the cell surface. *J. Biol. Chem.* **284**, 22481–22490 (2009).

41. Brasaemle, D. & Attie, A. Rapid intracellular transport of LDL-derived cholesterol to the plasma membrane in cultured fibroblasts - PubMed. *J. Lipid Res.* **31**, 103–12 (1990).

42. Neufeld, E. B. *et al.* Intracellular trafficking of cholesterol monitored with a cyclodextrin. *J. Biol. Chem.* **271**, 21604–21613 (1996).

43. Das, A., Brown, M. S., Anderson, D. D., Goldstein, J. L. & Radhakrishnan, A. Three pools of plasma membrane cholesterol and their relation to cholesterol homeostasis. *Elife* **3**, e02882 (2014).

44. Fielding, C. J., Bist, A. & Fielding, P. E. Intracellular Cholesterol Transport in Synchronized Human Skin Fibroblasts†. *Biochemistry* **38**, 2506–2513 (1999).

45. Elbadawy, H. M., Borthwick, F., Wright, C., Martin, P. E. & Graham, A. Cytosolic StAR-related lipid transfer domain 4 (STARD4) protein influences keratinocyte lipid phenotype and differentiation status. *Br. J. Dermatol.* **164**, 628–632 (2011).

46. Reynier, M. *et al.* Rab11a Is Essential for Lamellar Body Biogenesis in the Human Epidermis. *J. Invest. Dermatol.* **136**, 1199–1209 (2016).

47. Reynier, M. *et al.* The Actin-Based Motor Myosin Vb Is Crucial to Maintain Epidermal Barrier Integrity. *J. Invest. Dermatol.* **139**, 1430–1438 (2019).

48. Carton-Garcia, F. *et al.* Myo5b knockout mice as a model of microvillus inclusion disease. *Sci. Rep.* **5**, (2015).

49. Fabry, B., Klemm, A. H., Kienle, S., Schä, T. E. & Goldmann, W. H. Focal Adhesion Kinase Stabilizes the Cytoskeleton. (2011) doi:10.1016/j.bpj.2011.09.043.

50. Marinkovich, M. P. Laminin 332 in squamous-cell carcinoma. *Nat. Rev. Cancer 2007 75* **7**, 370–380 (2007).

51. Krueger, J. G., Lin, A. N., Leong, I. & Carter, D. M. Junctional Epidermolysis Bullosa Keratinocytes in Culture Display Adhesive, Structural, and Functional Abnormalities. *J. Investig. Dermatology* **97**, 849–861 (1991).

52. Jonkman, M. F., de Jong, M. C. J. M., Heeres, K. & Sonnenberg, A. Expression of

integrin α6β4 in functional epidermolysis bullosa. *J. Invest. Dermatol.* **99**, 489–496 (1992).

53. Robbins, P. B. *et al.* In vivo restoration of laminin 5β3 expression and function in junctional epidermolysis bullosa. *Proc. Natl. Acad. Sci. U. S. A.* **98**, 5193–5198 (2001).

54. Marinkovich, M. P., Keene, D. R., Rimberg, C. S. & Burgeson, R. E. Cellular origin of the dermal-epidermal basement membrane. *Dev. Dyn.* **197**, 255–267 (1993).

55. Ryan, M. C., Lee, K., Miyashita, Y. & Carter, W. G. Targeted disruption of the LAMA3 gene in mice reveals abnormalities in survival and late stage differentiation of epithelial cells. *J. Cell Biol.* **145**, 1309–1323 (1999).

56. Tayem, R. *et al.* Laminin 332 Is Indispensable for Homeostatic Epidermal Differentiation Programs. *J. Invest. Dermatol.* **141**, 2602-2610.e3 (2021).

57. Yuen, W. Y. *et al.* Long-term follow-up of patients with Herlitz-type junctional epidermolysis bullosa. *Br. J. Dermatol.* **167**, 374–382 (2012).

58. Hirsch, T. *et al.* Regeneration of the entire human epidermis using transgenic stem cells. *Nature* **551**, 327–332 (2017).

59. Singh, K. *et al.* JunB defines functional and structural integrity of the epidermo-pilosebaceous unit in the skin. *Nat. Commun.* **9**, 3425 (2018).

60. Ludovici, M. *et al.* Influence of the sebaceous gland density on the stratum corneum lipidome. *Sci. Rep.* **8**, 11500 (2018).

Funding

This work was supported by a British Skin Foundation grant.

Competing Interests statement

The authors declare there are no competing interests.

Figures

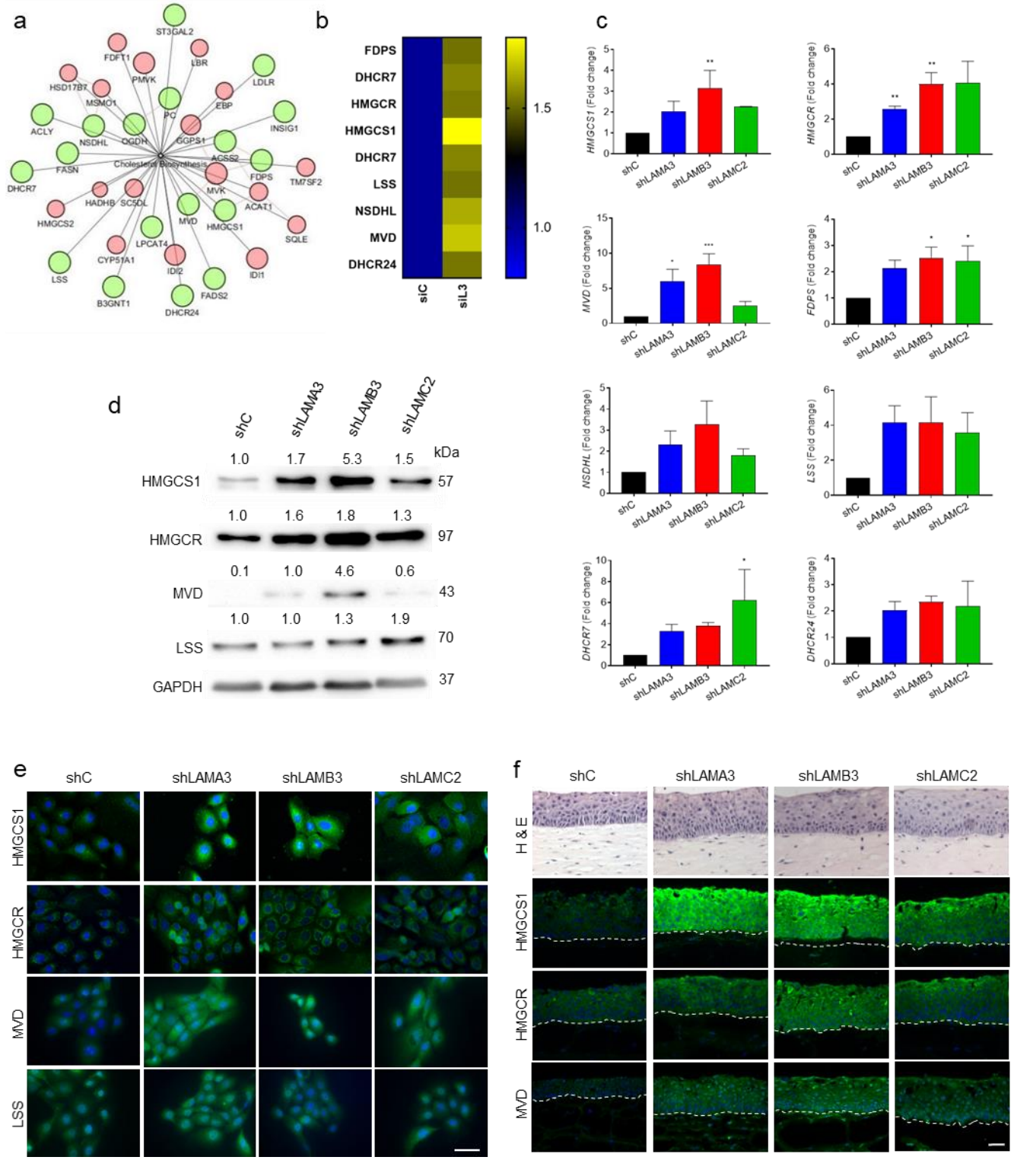

Figure 1. Loss of Laminin332 upregulates Cholesterol biosynthesis genes.

a) DAVID clustering analysis of RNA sequencing data for siLamA3 gene knockdown. **b)** Fold change of cholesterol biosynthesis genes with loss of basement membrane protein Lam332. **c)** Real-time quantitative reverse transcription analysis of cholesterol biosynthesis genes in Laminin332 knockdown cells. Statistical analysis was performed using one-way ANOVA and compared to shC. *p<0.05, **p<0.01, ***p<0.001. **d)** Western blotting analysis of HMGCS1, HMGCR, MVD and LSS in control (shC) and Lam332 knockdown (shLamA3, shLamB3, shLamC2) cells. GAPDH was used as an internal control of protein loading. For densitometry analysis, results were normalized to GAPDH and are expressed as fold induction over shC. **e)** Immunofluorescence staining of HMGCS1, HMGCR, MVD and LSS in cells (scale bar = 50µm). **f)** Haematoxylin & eosin and immunofluorescence staining of HMGCS1, HMGCR and MVD in 3D skin equivalents (scale bar = 50µm).

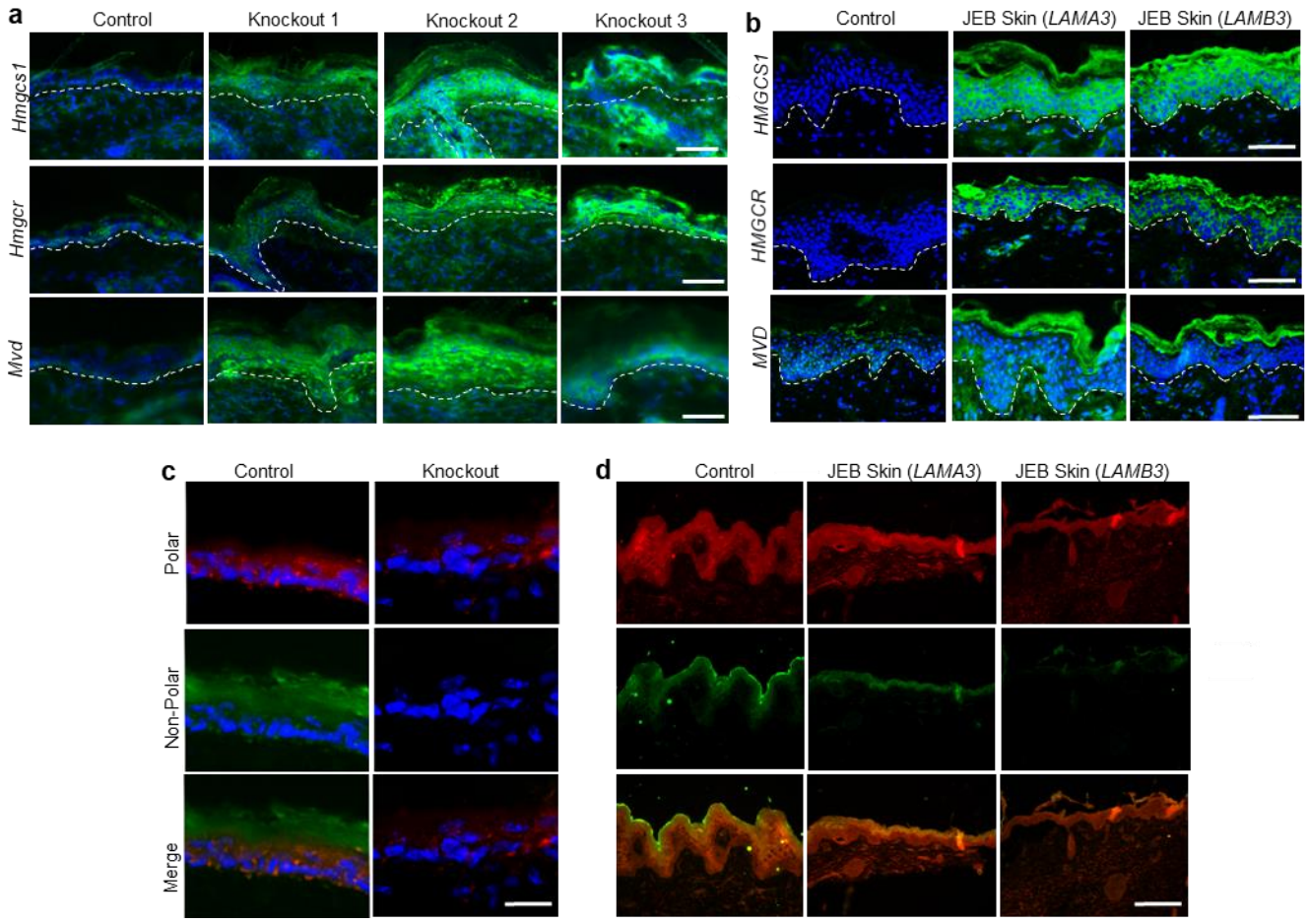

Figure 2. Cholesterol biosynthesis and lipid changes in *Lama3*$^{flox/flox}$/K14-CreERT mouse and JEB patient skin.

a) Immunofluorescence staining of cholesterol biosynthesis genes were performed in skin samples of a tamoxifen-treated heterozygous *Lama3*$^{wt/flox}$/K14-CreERT (control) mouse and *Lama3*$^{flox/flox}$/K14-CreERT (knockout). **b)** Representative images of control skin and JEB patient skin (with both *LAMA3* and *LAMB3* mutations stained for cholesterol biosynthesis. The lipid fluorescent stain Nile Red used to show both polar (red) and non-polar (green) lipids in **c)** mouse and **d)** JEB patient skin. Dotted line delineates the epidermis and dermis. DAPI (4',6-

diamidino-2-phenylindole) was used as a nuclear stain. Images shown are representative of 6 mice per group. JEB patient samples representative of 6 patients (3 with *LAMA3* mutation and 3 with *LAMB3* mutation). Scale bar = 50 µm

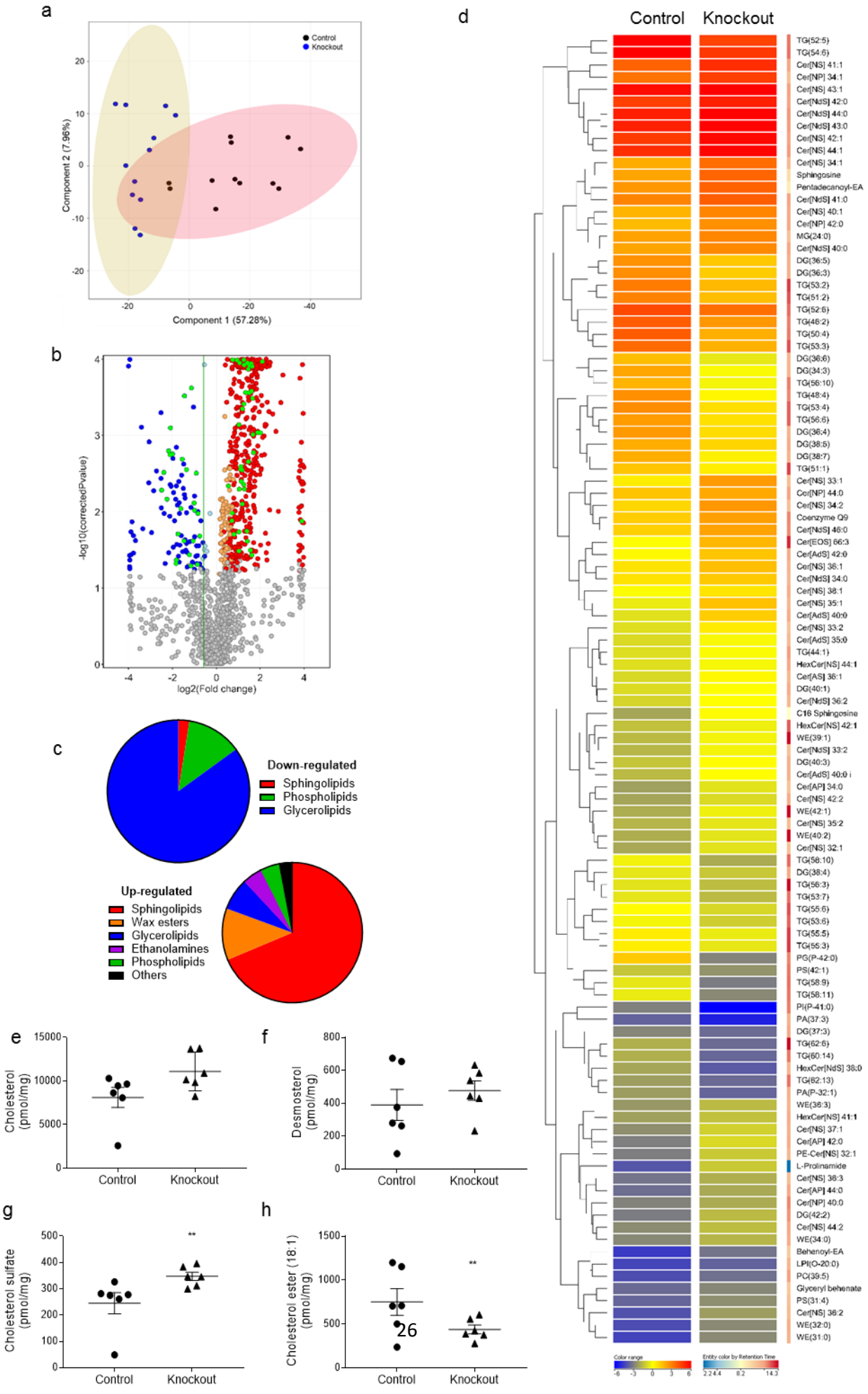

Figure 3. Lipidomic analysis of *Lama3*$^{flox/flox}$/K14-CreERT mouse.

Analysis from positive ion mode (+ESI). **a)** Principal component analysis (PCA) illustrating the variances between the two sample groups. Within the first two principal components 65.24% of the total variance was explained, with 57.28% in the first dimension and an additional 7.96% in the second dimension. **b)** Volcano plot analysis displaying significantly different regulated lipid species between Lama3 KO mice vs Control (Ctrl). The log2 of the fold change (FC) values were plotted on the x-axis, whereas the −log10 of the t-test p-values were plotted on the y-axis. The dots corresponding to each entity were coloured according to the FC, with red indicating significantly upregulated lipids and blue indicating significantly downregulated (based on $p < 0.05$ and $FC > 1.5$); green dots highlight the 107 lipid molecules further analysed in figures c and d. **c)** Further analysis revealed the main lipid sub-groups down-regulated (sphingolipids, phospholipids and glycerolipids) or upregulated (sphingolipids, wax esters, glycerolipids, ethanolamines, phospholipids and others) in KO vs Ctrl mouse groups and **d)** Integrated hierarchical clustering analysis of 107 lipid species through targeted MS/MS which were significantly different with a FC >1.5 between KO and Ctrl. Ceramide and triglyceride annotations were confirmed upon generation of MS/MS spectra. Colour scale (solid blue to solid red) reflects Log 2 values and colour scale (blue to red) shows retention time in the LC-MS analysis indicated in minutes. **e-h)** Quantitative analysis of cholesterol related lipid species cholesterol, desmosterol (with GC-MS), cholesterol sulfate and CE(18:1) (with LC-MS) respectively. Statistical analysis was performed using an unpaired t-test $^{**}p < 0.01$ ($n = 6$).

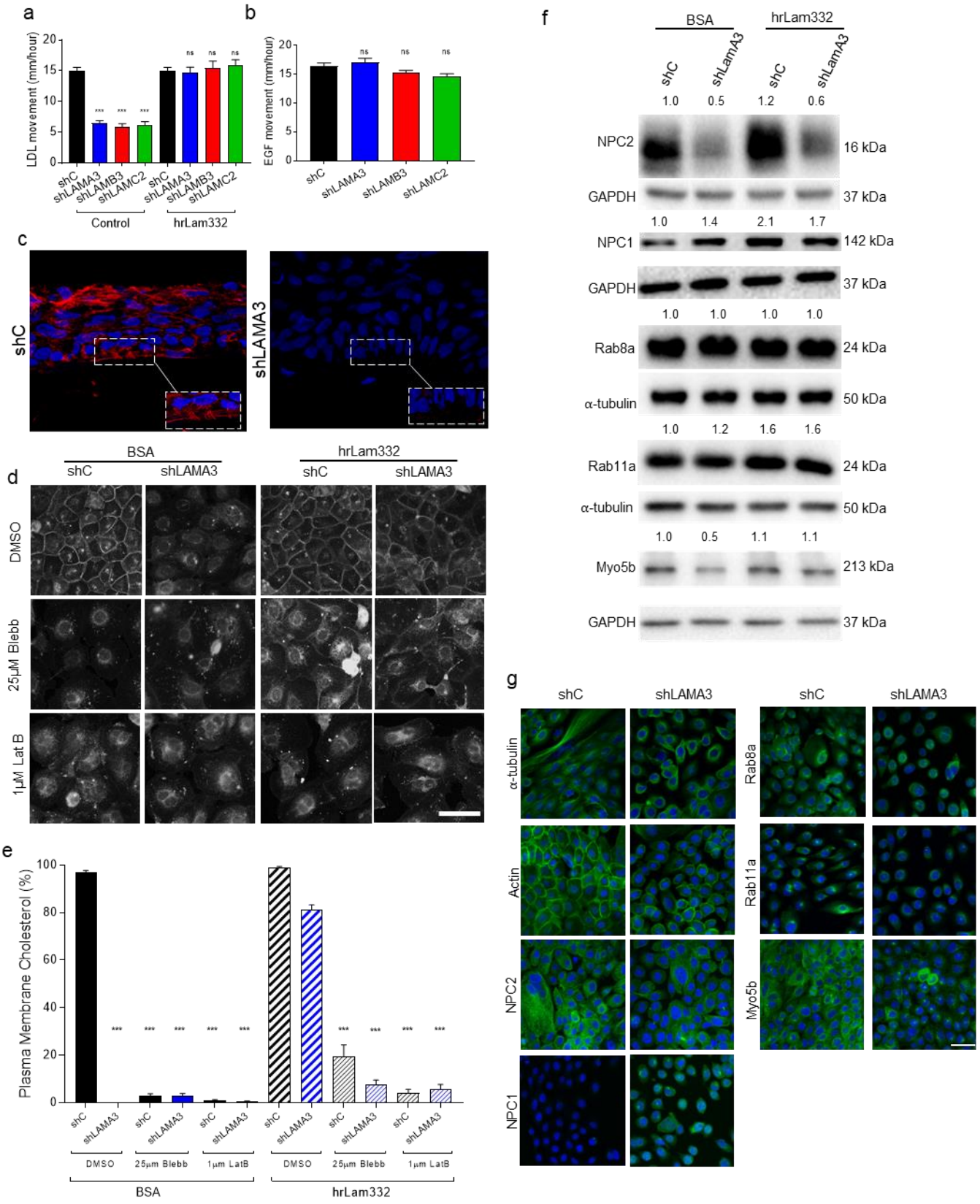

Figure 4. Cellular quantification and localisation of cholesterol with loss of Laminin332.

a) Quantification of movement of fluorescently labelled dil-LDL (1,1′-dioctadecyl-3,3,3′,3′-tetramethylindo-carbocynanine perchlorate-LDL) in control and Lam332 knockdown cells cultured on BSA or hrLam332. **b)** Trafficking of fluorescent EGF as a control was carried out in both shC and Lam332 knockdown cells showing no significant difference. Videos (20 of each condition) were quantified using particle tracking on ICY software and statistical analysis performed. **c)** Representative images for actin cytoskeleton staining both in control and shLamA3 3D skin equivalents showing significant loss of actin fibres at the basement membrane in Lam332 skin equivalents. The inset in each panel represents a closer view of the basement membrane region d**)** Fluorescent filipin staining (which binds to free cholesterol within the cell) in control and shLamA3 knockdown keratinocytes cultured on BSA or hrLam332, with and without Blebbistatin and Latrunculin B. **e)** Images were quantified and results presented as percentage of plasma membrane cholesterol. **f)** Western blotting analysis of cholesterol transport pathway genes (NPC2, NPC1, Rab8a, Rab11a and Myo5b) in control and shLamA3 knockdown cells cultured on BSA or hrLam332. **g)** Immunofluorescence of α-tubulin, actin, NPC2, NPC1, Rab8a, Rab11a and Myo5b in control and shLamA3 knockdown cells. Statistical analysis for all above experiments was performed using one-way ANOVA, *p<0.05, **p<0.01 and ***p<0.001. Scale bar 50µm.